Normal Molecular Repair Mechanisms in Regenerative Peripheral Nerve Interfaces Allow Recording of Early Spike Activity Despite Immature Myelination

Jennifer L. Seifert, Vidhi Desai, Robert C. Watson, Tabassum Musa, Young-tae Kim, Edward W. Keefer, and Mario I. Romero, *Member, IEEE*

***Abstract*—Clinical use of neurally controlled prosthetics has advanced in recent years, but limitations still remain, including lacking fine motor control and sensory feedback. Indwelling multi-electrode arrays, cuff electrodes, and regenerative sieve electrodes have been reported to serve as peripheral neural interfaces, though long-term stability of the nerve–electrode interface has remained a formidable challenge. We recently developed a regenerative multi-electrode interface (REMI) that is able to record neural activity as early as seven days post-implantation. While this activity might represent normal neural depolarization during axonal regrowth, it can also be the result of altered nerve regeneration around the REMI. This study evaluated high-throughput expression levels of 84 genes involved in nerve injury and repair, and the histological changes that occur in parallel to this early neural activity. Animals exhibiting spike activity increased from 29% to 57% from 7 to 14 days following REMI implantation with a corresponding increase in firing rate of 113%. Two weeks after implantation, numbers of neurofilament-positive axons in the control and REMI implanted nerves were comparable, and in both cases the number of myelinated axons was low. During this time, expression levels of genes related to nerve injury and repair were similar in regenerated nerves, both in the presence or absence of the electrode array. Together, these results indicate that the early neural activity is intrinsic to the regenerating axons, and not induced by the REMI neurointerface.**

***Index Terms*—Multi-electrode arrays, myelin, nerve regeneration, neural recording, PCR microarrays, peripheral nerve interfacing.**

Manuscript received May 01, 2011; revised October 04, 2011; accepted November 27, 2011. Date of publication December 23, 2011; date of current version March 16, 2012. This work was sponsored by The Defense Advanced Research Projects Agency (government contract/grant number N66001-11-1-4408). The views, opinions, and/or findings contained in this article are those of the author and should not be interpreted as representing the official views or policies, either expressed or implied, of the Defense Advanced Research Projects Agency or the Department of Defense.

J. L. Seifert, V. Desai, R. C. Watson, Y. Kim, and M. I. Romero are with the University of Texas at Arlington, Arlington, TX 76010 USA (e-mail: jenseifert@uta.edu; vidhi.desai@mavs.uta.edu; robert.watson@mavs.uta.edu; ykim@uta.edu; mromero@uta.edu).

T. Musa and E. W. Keefer are with Plexon, Inc., Dallas, TX 75206 USA (e-mail: tabassum@plexon.com; edk@plexon.com).

Color versions of one or more of the figures in this paper are available online at http://ieeexplore.ieee.org.

Digital Object Identifier 10.1109/TNSRE.2011.2179811

I. Introduction

In THE United States, there are approximately 1.7 million people living with limb loss [1], and it is estimated that one out of every 200 people in the U.S. has had an amputation, whether due to dysvascular complications, trauma, cancer, or congenital limb differences [2], [3]. While recent advances in robotics appear promising for the recovery of some function through the use of prosthetics, neural control of these devices remains incomplete and unreliable. The limitations of nerve electrode interfaces vary depending on the type of electrode and the response of the implantation tissue, however, signal decay over time has remained an insurmountable challenge despite the multiple electrode technologies available [4]–[6].

Current clinical alternatives through the use of electromyographic signals from reinnervated pectoral muscles, allow the control robotic prosthetics with some success, though motor control is limited to gross voluntary movements and sensory feedback is lacking or incomplete [7]–[9]. Fine motor control and sensory function will require more extensive integration between the nervous system and implantable electronics. Recent advances in electrode designs have moved away from extraneural cuff and extrafascicular electrodes which provide a low number of small signals [10], [11] and instead have focused on penetrating electrodes. Indwelling arrays have been studied extensively in cortical implantations and have shown the ability to provide some level of manual dexterity [12], [13] and cortical stimulation of sensory areas has also yielded some spatiotemporal feedback in primates [14]. While these pursuits have produced promising, if not long lasting, results, the invasiveness of cortical implantation is an obstacle to clinical implementation. As such, investigators have more recently evaluated the feasibility of interfacing with residual sensory and motor activity in the peripheral nervous system (PNS) of amputees [13], [15]–[17].

Penetrating electrodes in the PNS can provide both a high number and better quality of action potential recordings but still have many limitations, which lead to signal decay. These include poor tissue–electrode interface, tissue damage by probe micromotion within the soft nerve tissue, and electrode insulation due to tissue scar formation [18]–[21]. We recently reported that peripheral nerves, whether acutely injured or implanted after months of chronic amputation, could be interfaced

1534-4320/$26.00 © 2011 IEEE

early by enticing them to grow in close proximity to electrodes placed in a tridimensional open regenerative multielectrode interface (REMI) [22]. The REMI was able to detect signals as early as eight days post-implantation; however nerve regeneration during the first two weeks is dynamic thus, the REMI early recorded activity is expected to be highly variable as well. While this activity might represent normal neural depolarization during axonal regrowth, it is also possible that the recorded action potentials are the result of altered nerve regeneration in the presence of REMI electrodes.

Nerve injury leads to the rapid influx of signals that contribute to cellular injury and stress followed by the induction of transcription factors, adhesion molecules, growth-associated proteins and structural components needed for axonal elongation [23]. Efforts to evaluate the foreign body response at neural interfaces have been limited to quantification of a small set of molecules *in vitro* (i.e., MCP-1, TNF-α, IL-1b, and IL-6) [20] and *in vivo* (i.e., ED-1, GFAP) [24]. Quantification of gene expression changes during *in-vivo* electrode implantation has not been evaluated and thus molecular components and pathways crucial for the immune response to neural interfaces remain largely unknown. In the present study we evaluated high-throughput expression levels of 84 specific genes related to nerve injury repair and the quality of axonal regeneration and remyelination. In the first two weeks post-injury, we determined whether the REMI interferes with the regenerative process and provide a molecular and histological framework to understand the early neural activity recorded using the REMI peripheral neural interfaces.

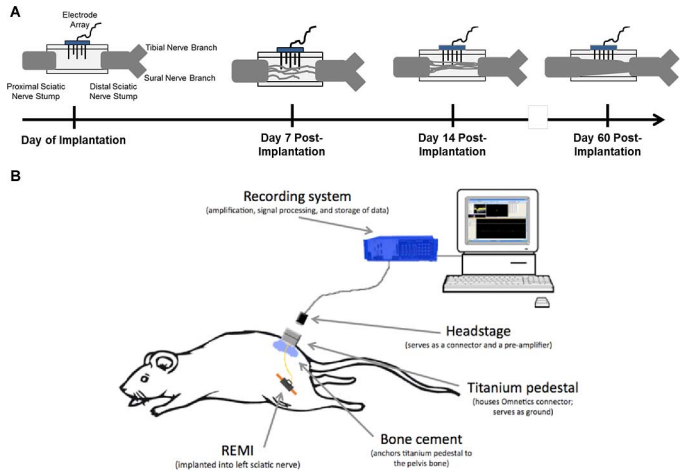

Fig. 1. (A) Schematic of the REMI implantation design and timeline of observed degree of regeneration through the REMI. (B) Wiring diagram depicting the recording setup for acquiring electrophysiological signals.

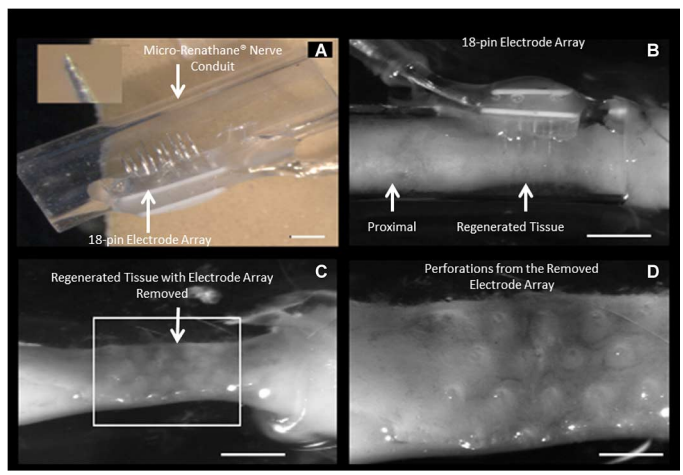

Fig. 2. (A) Photograph of the REMI, an 18 pin multi-electrode array mounted in a tubular nerve guide. The insert shows a higher magnification picture of a single electrode. (B) Normal nerve regeneration is observed through the electrode-conduit assembly 15 days post-implantation. (C, D) Removal from the REMI revealed nerve tissue growth across the electrode array, as well as clear perforations observed after its removal. Scale bar = 2 mm (A), 1 mm (B, C), and 500 μm (D).

II. Methods

A. Regenerative Multielectrode Interface (REMI)

Custom-made floating arrays with 18-pin Parylene-C insulated platinum/iridium electrodes were used (150–300 kΩ impedance at 1 kHz, Microprobes Inc., Gaithersburg, MD). Individual electrodes were approximately 50 μm in diameter at the shank, varied in height (0.7–1.0 mm), and were placed 400 μm apart to maximize contact with the regenerating nerve fibers [Fig. 2(a)]. The array cable was fabricated from Parylene-C insulated 25-μm gold wires wound in a helix and coated with a NuSil-type MED6-6606 nonrestrictive silicone elastomer and was 4.5 cm in length. The cable was sonically bound to an Omnetics connector (Minneapolis, MN), housed in a titanium pedestal. Microarrays were placed in the lumen of polyurethane nerve guide tubes (Micro-Renathane, Braintree Scientific, Inc., Braintree, MA; OD 3 mm, ID 1.75 mm, and 7 mm in length). The entire assembly was sterilized and the lumen filled with collagen I/III (0.3%; Chemicon, Temecula, CA) prior to surgery.

B. Surgical Procedure

Thirty female Lewis rats (215–275 g) were used for this study. The animals were divided into the following four groups: Control (15 days after tubularization nerve repair) groups for PCR (1; $n = 6$) and histology (2; $n = 7$), and experimental groups (15 days after REMI implantation) for PCR (3; $n = 6$); and histological studies (4; $n = 11$). The animals were anesthetized with isoflurane (5% induction, 2%–2.5% maintenance) in 100% oxygen. When an adequate depth of anesthesia was attained (loss of corneal reflex), the shaved dorsal surface was cleaned with povidone-iodine. The sciatic nerve was exposed through a muscle-sparing incision along the sciatic vein between the semitendinosus and the biceps muscles. The two muscles were gently spread to expose the proximal part of the undivided nerve, which was then transected. The proximal and distal nerve stumps were introduced into opposite ends of a sterile tube or REMI, and sutured in place [Fig. 1(a)]. The electrode array within the REMI is connected to an 18-pin connector via subcutaneous gold microwires. The connector, housed in a silicone-sealed titanium pedestal was mounted to the pelvis with bone cement (Biomet; Warsaw, IN). In order to obtain a clean, flat surface on which to adhere the pedestal, an incision was made above L5-S2. The fascia was cut and

reflected and the underlying muscle tissue removed to expose the dorsal processes and the pelvic bone. The tips of each exposed dorsal process were removed and the pelvic bone was cleaned and dried. The bone cement was then mixed according to manufacturer's instructions and applied to the pelvis, creating a flat platform on which to place the pedestal. More bone cement was added around the pedestal to hold it in place. The skin was then closed around the pedestal using staples. Control animals underwent the same surgical procedure with the exception being that the collagen filled tube did not contain an electrode array. All animals received antibiotic (cephazolin; 5 mg/kg, IM) and pain control (buprenorphine; 0.05–0.1 mg/kg, SC) treatment post-surgery. All procedures were performed in accordance with the guidelines of the Institutional Animal Care and Use Committee of the University of Texas at Arlington.

C. Electrophysiological Recordings

Electrophysiological signals, from seven freely moving rats, were recorded with the OmniPlex data acquisition system (Plexon Inc., Dallas, TX) at the seventh and fourteenth day postsurgical implantation. Offline Sorter software (Plexon) was used to sort the neural spikes by threshold detection and principal component analysis. The sorted spikes were then analyzed using NeuroExplorer (Nex Technologies, Westford, MA) and MATLAB to quantify the amplitude of spikes using Peak Detection, number of spikes, and firing rate. A wiring diagram depicting the recording setup is shown in Fig. 1(b).

D. Total RNA isolation and quantitative RT-PCR:

Twelve animals (six control and six experimental) were sacrificed at 15 days post-implantation and the harvested regenerated sciatic nerve was immediately preserved in RNA Later (Qiagen, Valencia, CA). Total RNA from regenerated tissue was extracted with Qiazol and purified using RNeasy Micro kit (Qiagen). RNA purity was verified by obtaining optical densitometry readings at 260/280 nm, as well as at 260/230 nm. 1 μg of total RNA was converted to cDNA using RT First strand kit (SABiosciences, Frederick, MD). PCR amplifications were performed using Mx3005P qPCR instrument (Agilent Technologies, Santa Clara, CA) on 96 well custom PCR arrays (SABiosciences) consisting of 84 genes of interest including surface molecules (CD28, CD34, CD3D, CD3E, CD3G, CD4, CD40LG, CD8A, ICAM1, ICOS, ISG20), chemokines (CCL1, CCL2, CCL20, CCL22, CCL7, CD247, CX3CL1, CXCL1, CXCL12, CXCL2, CXCL5, CXCL6, IL8, MMP13, MMP3, MMP9), cytokines (CSF2, CSF3, IFNG, IL10, IL12B, IL13, IL15, IL17A, IL17C, IL17D, IL17F, IL18, IL1B, IL2, IL21, IL22, IL23A, IL25, IL27, IL3, IL4, IL5, IL6, TGFB1, TNF), and cytokine receptors (IL12RB1, IL12RB2, IL17RB, IL17RC, IL17RD, IL17RE, IL23R, IL6R, IL7R). Other genes included some transcription factors, housekeeping genes, gDNA control, reverse transcript controls, and positive PCR controls. Relative regulation values were determined using a $\Delta\Delta\mathrm{Ct}$ formula.

E. Histological Analysis

Two weeks after implantation, the animals were sacrificed with an overdose injection of sodium pentobarbital (100 mg/kg; IP) followed by transcardial perfusion with 0.9% saline for 5 min and 4% paraformaldehyde for 15 min. The sciatic nerve containing tubes [both control ($n = 7$) and electrode implanted ($n = 11$)] were harvested and post-fixed overnight in 4% paraformaldehyde [Fig. 2(b)]. After removal from the tubing [Fig. 2(c) and (d)], the sciatic nerve was processed for paraffin embedding and sliced (horizontal, 6 μm) for immunohistological analysis. The sliced tissues were triple immunostained for regenerating axons (NF200 or NF160, Rb IgG, 1:200, Sigma), myelination (Protein zero, Ch IgY, 1:200, Millipore) and macrophages (ED-1, mIgG1, 1:500, AbD Serotec). Secondary antibodies were diluted 1:220 in 0.5% triton in PBS and included goat anti-rabbit IgG Dylight 488 (Jackson Immunoresearch) for NF200 or 160, goat anti-mouse IgG1 Alexa 350 (Invitrogen) for ED-1 and goat anti-Chicken IgY Dylight 594 (Jackson Immunoresearch) for Protein zero. Animals without REMI, but the same injury and nerve regeneration via the same tube, were used as a control.

III. Results

A. The REMI Does Not Alter Early Nerve Regeneration

To evaluate the regenerative capacity of the REMI, the sciatic nerve was harvested two weeks after implantation and the tissue examined for gross anatomical characteristics [Fig. 2]. As previously reported for 21 days after injury, nerve regeneration across the REMI appeared robust with many of the electrodes firmly embedded in the tissue [Fig. 2(b)]. Perforations made by the electrodes were clearly visible upon removal of the electrodes from the tissue [Fig. 2(c) and (d)].

In order to determine the cellular composition of the regenerating tissue within the nerve conduit, immunostaining was utilized to evaluate axons and macrophages. Regenerated large diameter axon fibers immunolabeled for neurofilament 200 (NF200), were observed throughout the nerve gap in the simple tube [Fig. 3(a)] and across the electrode array in the REMI implanted animals [Fig. 3(b)]. At this early time, most of the electrodes in the REMI were clearly embedded in the tissue, and no difference was observed in the apparent density of regenerated axons. To evaluate the inflammatory response elicited by the natural process of nerve injury and repair, and to ascertain the possibility of an enhanced immune response elicited by the REMI, we immunolabeled ED1+ macrophages [Fig. 3(c) and (d)]. These cells were enriched at the proximal and distal ends of the regenerated nerves. However, while macrophages in the control tissue appeared to be more evenly dispersed [Fig. 3(c)], those in the REMI were observed encircling the perforations left by the electrodes [Fig. 2(d)].

To ascertain if the regenerated tissue was completely remyelinated at 15 days, and to determine if REMI electrodes interfere in this process we immunostained the tissue for protein zero (P0), a major structural component of peripheral myelin [Fig. 4(a) and (b)]. Myelin was observed in both the control [Fig. 4(a)] and the REMI implanted tissue [Fig. 4(b)] at comparable levels. However, and in contrast to the NF-200 staining, the distribution of P0-positive axons is more abundant in the proximal ends and diminishes in the middle of the regenerate. This result revealed a degree of immaturity in the remyelination process at 15 days post-injury, and one that appears to follow

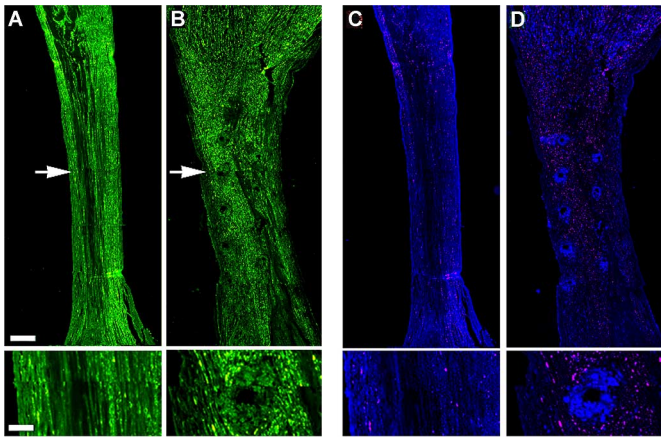

Fig. 3. Immunolabeling of injured nerve tissue using the axonal marker NF200, (A, B, green) 15 days post-repair using either a simple tube (A, C) or a REMI (B, D), shows comparable axonal growth across the nerve gap in both repair methods. Visualization of ED-1-postive macrophages (C, D, blue) demonstrated a high concentration of these cells at the proximal and distal ends of both types of regenerated nerves, and around each REMI electrode. The arrows indicate areas in A–D, shown at higher magnifications in the bottom photographs of each picture. Scale bars $= 200\ \mu$m (top), 55 μm (bottom).

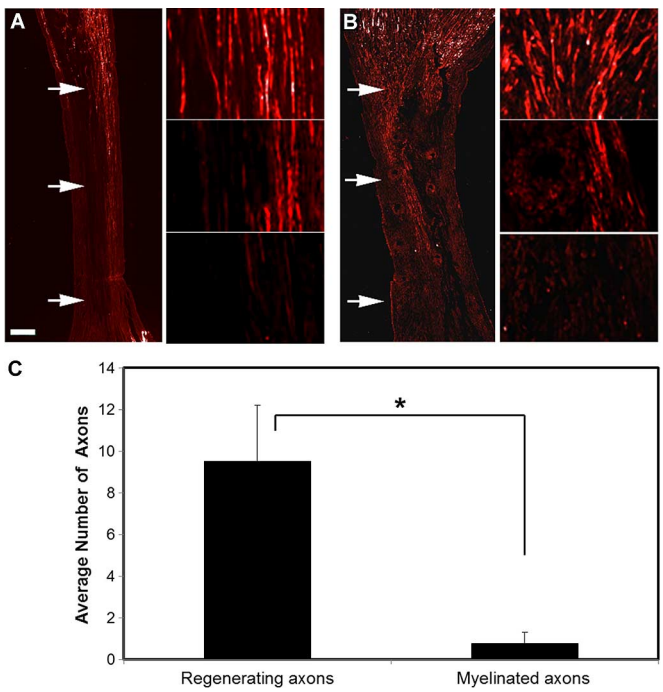

Fig. 4. Immunocytochemical visualization of myelin using the Protein zero marker, revealed that only a small fraction of the large-diameter axons regenerated across the gap (A) and through the REMI (B), are remyelinated at 15 days after injury. The arrows indicate proximal (top), middle, and distal (bottom) areas, in both the control and REMI regenerated nerve, shown at higher magnification in the respective inserts. Remyelination proceeds in a proximo-distal gradient and is at a rather immature stage 15 days after nerve injury. Scale bars $= 200\ \mu$m A, B (large pictures) and 35 μm (inserts). Quantification of total number of axons and number of myelinated axons is shown in C ($n = 11$; $*$ indicates $p < 0.0001$).

the initial robust axonal regeneration. Quantification of the total number of axons and the number of myelinated axons within a 100 μm area around each embedded electrode supports this observation [Fig. 4(c)]. They also show a highly dynamic cellular

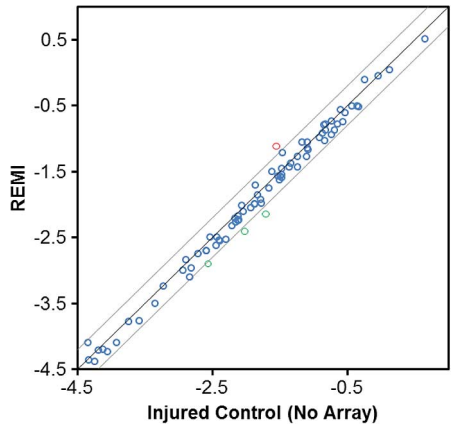

Fig. 5. Scatter plot of relative expression of 84 genes in the regenerated sciatic nerve 15 days post-injury through a nerve conduit without an electrode array (Group 1, X-axis) and with an electrode array (Group 2, Y-axis). [Two fold up (o)/down (o) regulation of gene of interest] ($n = 6$ per group).

environment that takes place in the first two weeks of REMI implantation, with NF200 labeling showing robust nerve regeneration not altered by the electrodes, the ED-1 staining suggested an immediate immune response towards the REMI electrodes, and the P0 revealing partial remyelination at this time post-injury. Since the images are qualitative and limited in molecular scope, we decided to evaluate the nerve regeneration through the control and REMI nerves using a high-throughput PCR gene microarray study.

B. Similar Gene Expression Profiles of Regenerated Tissue in the Presence or Absence of an Electrode Array

After 15 days post-injury, gene regulation of all 84 genes assayed in groups with and without electrode arrays were roughly identical (Fig. 5). In the presence of the electrode array, metalloprotease-3 (Mmp3, fold change 2.7) was up regulated, and glial-derived neurotrophic factor (GDNF, -2.1), neuregulin-1 (Nrg1, -2.4), and nestin (Nes, -2.5) were down regulated. Notably, the expression levels of macrophage markers were not upregulated in the electrode-implanted tissue.

Also, similar changes in genes related to nerve injury and nerve regulation were observed in both groups (i.e., regeneration with or without an electrode array) in comparison to uninjured nerve controls (Fig. 6). The up regulation of genes related to nerve growth factors, Schwann cells, cell regulators and cell adhesion molecules, and down regulation of genes related to mature Schwann cells and neurotransmitters appeared consistent in both groups as compared to uninjured nerve tissue. The genes with changes in expression levels as compared to uninjured nerves are included in Table I. These results indicate that the presence of the electrode array in the nerve conduit does not alter the molecular mechanisms of regeneration and that, as expected, the gene regulation profile in the regenerating sciatic nerve is different from that of uninjured tissue.

C. Increasing Signals from 7 to 14 Days Following REMI Implantation

In order to evaluate the capacity of the regenerating sciatic nerve to conduct nerve potentials at early time points, we

TABLE I
RELATIVE GENE EXPRESSION IN SCIATIC NERVE REGENERATED IN THE PRESENCE AND ABSENCE OF ELECTRODE ARRAY COMPARED TO UNINJURED SCIATIC NERVES. GENES OF INTEREST INCLUDED HERE WERE EITHER UP- OR DOWN-REGULATED BY AT LEAST TWO FOLD

	Up regulated Genes					Down regulated Genes			
	Wound healing/ Inflammatory	Progenitor/ Neural Crest/ Stem Cell	Stress Signaling	Neuotrophins/ Receptors	ECM remodeling and Axon guidance	Stress Signaling	Neuotrophins/ Receptors	Schwann Cell Markers	ECM remodeling and Axon guidance
Without electrode Array	Cxcr4, Tgfb1, Tgfbr1, Cd68, Tnf	Cd40, Thy1, Bmp1, Sox10	Ctnnb1 Faslg, Pik3cg, Hmox1 Tp53 Nfkb1	Lif, Gdnf Bdnf, Ngf Nrg1, Pdgfb Ngfr	Fn1, Tnc, Mmp3, Mmp9, Plat, Ncam1, Igtb1, Unc5a	Pparg	Ntrk2, Egf	Cntf, Mbp, Gfap S100b	Dcc
With electrode Array	Cxcr4, Tgfb1, Tgfbr1, Cd68	Cd40, Thy1	Ctnnb1 Faslg, Pik3cg, Hmox1 Tp53	Lif, Gdnf Bdnf, Ngf Nrg1, Pdgfb Ngfr	Fn1, Tnc, Mmp3, Mmp9, Plat, Ncam1	Pparg	Ntrk2, Egf	Cntf, Mbp, Gfap S100b	Ntn1, Dcc

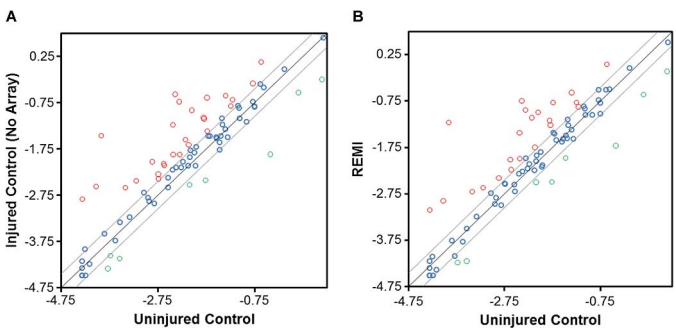

Fig. 6. (A) Scatter plot of relative expression of 84 genes in an uninjured sciatic nerve (Control Group, X-axis) and a regenerated sciatic nerve 15 days post-injury through a nerve conduit without an electrode array (Group 1, Y-axis). (B) Scatter plot of relative expression of 84 genes in an uninjured sciatic nerve (Control Group, X-axis) and a regenerated sciatic nerve 15 days post-injury through a nerve conduit with an electrode array (Group 2, Y-axis). [Two fold up (o)/down (o) regulation of gene of interest] ($n = 6$ per group).

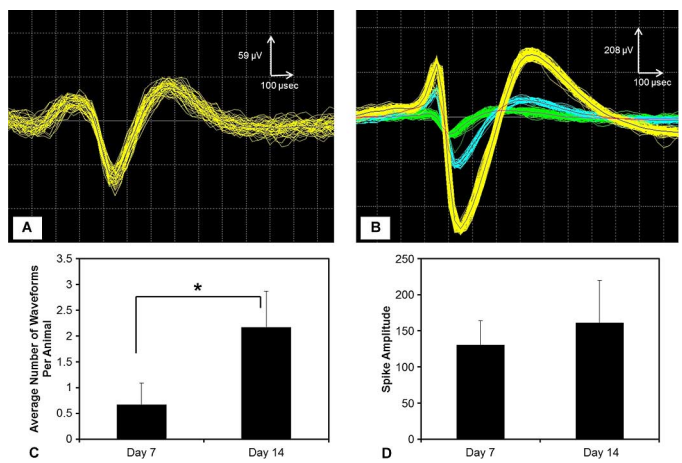

Fig. 7. (A) Sample single-unit recording from an animal seven days post-implantation. (B) Sample multiunit recording from an animal 14 days post-implantation. (C) Average number of observable distinct single-unit waveforms detected on day 7 and day 14 post-implantation ($n = 7$; data are represented as mean $+/-$ SEM). (D) The average amplitude across all animals did not change significantly from day 7 to day 14 recordings ($n = 7$; $*$ indicates $p \leq 0.05$).

recorded from seven REMI-implanted animals, while awake, at 7 and 14 days post-implantation. Single spike activity was observed in 2/7 (29%) of animals at 7 days and in 4/7 (57%) at 14 days. Noise levels remained relatively stable at approximately 20–30 μV. In animals with single spike activity, the number of channels recording single units was 4 at day 7, and increased to 11 channels at 14 days. Action potentials measured up to 215 μV on day 7 and as large as 814 μV on day 14. Samples of a single-unit waveform from day 7 and a multiple-unit recording from day 14 are shown in Fig. 7(a) and (b), respectively. Overall, the number of observable, single-unit waveforms increased significantly by 225% from day 7 to day 14 [$p \leq 0.05$; Fig. 7(c)] and the average signal amplitude increased, albeit not significantly from 130 to 161 μV from the first to the second week [Fig. 7(d)]. Sample raster plots from the same animal on day 7 and 14 are shown in Fig. 8(a) and (b) to illustrate changes in firing patterns over this early time after REMI implantation. The average number of single spikes detected per minute increased significantly by 113% from day 7 to 14 [$p \leq 0.05$; Fig. 8(c)].

Taken together, these results demonstrate that the regenerating nerves growing through the multielectrode array during the first two weeks post-implantation are electrically active. While the percentage of animals with active recordings was still relatively low during the first week post-implantation, the neural activity gradually increases in the number, amplitude and frequency of the recorded neural spikes over the first 14

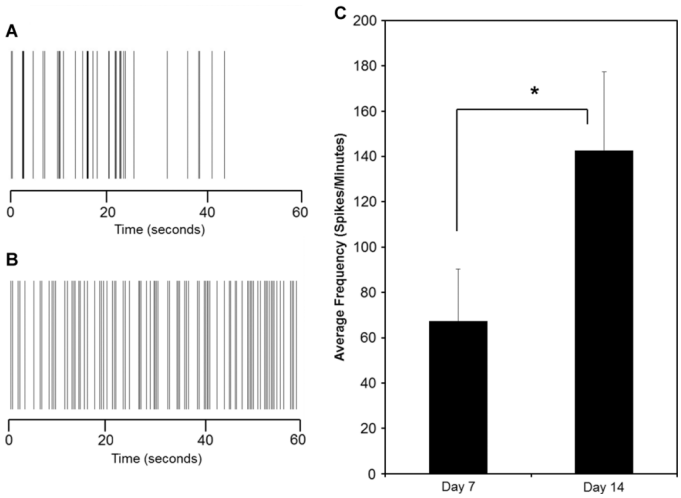

Fig. 8. (A) Representative raster plot from 1 min of a day 7 recording. (B) Representative raster plot from 1 min of a day 14 recording. (C) The number of recorded spikes per minute increased significantly from day 7 to day 14 post-implantation. Data are represented as mean $+/-$ SEM ($n = 7$; $*$ indicates $p \leq 0.05$).

days after peripheral neural interfacing. This trend is significant despite the fact that there is a presumably insulating layer of ED-1 positive macrophages encapsulating the electrodes, and that the process of remyelination is still immature.

IV. Discussion

We recently reported that peripheral nerves, whether acutely injured or implanted after months of chronic amputation, could be interfaced early by enticing them to grow in close proximity to electrodes placed in a tridimensional open regenerative multielectrode interface (REMI). The early neural activity was recorded at a time at which nerve regeneration is a dynamic interplay of cellular responses that include repair, immune and myelin reabsorbing cells, as well as vigorously regenerating axons. Here, we extended this work by looking in more detail at the neural activity recorded during the first two weeks of implantation, specifically investigating if the dynamic regenerative events at this early time post-injury are affected by the presence of the REMI electrodes.

During the first few weeks following transection, peripheral nerves undergo significant remodeling dependent upon the environmental milieu. Major contributors to the early microenvironment are Schwann cells and their precursors [25]. Proliferating Schwann cells form a scaffold along the basement membrane of approximated nerve stumps, a step that is critical for axonal elongation [26], [27]. Components of this important scaffold include laminin and fibronectin extracellular matrix proteins, as well as neurotrophins and other growth factors to entice regeneration. Inhibition of the formation of this Schwann cell scaffold, via blockage of proliferation, results in a greatly reduced capacity for regeneration [28]. An important signaling molecule, secreted by neurons, is neuregulin. This molecule is a signal that during the postnatal period instructs Schwann cells to myelinate axons [29]–[32] and, in an injured nerve, for the Schwann cells to demyelinate, dedifferentiate and begin to proliferate and secrete growth promoting and chemotactic factors [33].

In the present study we observed robust nerve regeneration in both control nerve gaps and those implanted with a REMI electrode array, as evidence by the visualization of NF-200 axons. As previously reported, the multielectrode array elicited a foreign-body response characterized by the encapsulation of the electrode by ED1+ macrophages. This is not unexpected as regenerative neurointerfaces are the most damaging and invasive neural interface method as they rely on the complete transection of the nerve. However, despite the formation of layers of presumably insulating cells around the electrodes, which have been implicated in the failure of most nerve–electrode interfaces, the electrical activity not only recorded in an increasing number of animals, but was clearly increasing in number and frequency of action potentials during the first two weeks after implantation. These data suggest that, in this neural interfacing method, factors other than the "cellular scar" around the electrodes may be responsible for the decay of the signal quality over time in regenerative neural interfaces.

One possible explanation for signal decay in the absence of increasing scar tissue is the increasing presence of myelinated axons at later stages of regeneration. In contrast to cortical neural interfaces, regenerative electrodes in the PNS are affected by the natural ability of the regenerated nerve for remyelination. The myelin sheath is a multilamellar membrane of high electrical resistance that covers axon segments of 500–1000 μm and functions as an insulator [34]–[36]. In injured peripheral nerves, remyelination initiates 2–3 weeks after the initial insult [34]. The extent to which remyelination affects the functioning of PNS interfaces is currently unknown. However, due to the high electrical resistance of the myelin sheet, remyelination is expected to dramatically diminish the electrical recording of action potentials if the electrode is surrounded by remyelinated axons.

The notion that the immune and inflammatory responses are not solely responsible for signal decay of implanted electrode arrays over time is also supported by our high-throughput gene expression profile analysis, which indicated that 84 genes, including those that are activated in inflammation, cell death, neural injury and repair, are comparable in REMI regenerated nerves and those expressed in control injured nerves. For decades, the decay in electrical signal activity has been evaluated primarily by electrophysiology. Solely analyzing one data set to evaluate such complex physiological responses can result in bias. In our study we resourced to a varied selection of tools including histological analysis, gene expression profiling, and electrophysiological evaluation to enrich the interpretation of the results. This complementary approach demonstrates that the presence of the REMI electrodes does not impair nerve regeneration, that the inflammatory response known to be critical in the nerve repair process occurs at rates comparable to control injured nerves and that the electrical activity of the extending axons increase over time during the first two weeks of neural interfacing.

This study also demonstrated that neural spike activity could be observed during times at which re-myelination of the regenerated nerve is immature. This can be explained if most of

the initially regenerating neurons are unmyelinated fibers. Alternatively, this result may suggest that regenerating, immature yet-to-be myelinated axons depolarize spontaneously.

In summary, this study demonstrates that the early electrical recording in regenerating peripheral nerves is inherently unstable due to the dynamic nerve growth and tissue repair ongoing during the first two weeks. However, the ability to observe increasing electrical activity over this time period, along with robust axonal regeneration around the electrodes lends credence to the notion that the REMI may provide a viable strategy for stable nerve–electrode interfaces as a means for prosthetic control.

REFERENCES

[1] K. Ziegler-Graham, E. J. MacKenzie, and P. L. Ephraim *et al.*, "Estimating the prevalence of limb loss in the United States: 2005 to 2050," *Arch. Phys. Med. Rehabil.*, vol. 89, no. 3, pp. 422–429, Mar. 2008.

[2] P. F. Adams, G. E. Hendershot, and M. A. Marano, "Current estimates from the National Health Interview Survey, 1996," *Vital Health Stat.*, vol. 10, no. 200, pp. 1–203, Oct. 1999.

[3] T. R. Dillingham, L. E. Pezzin, and E. J. MacKenzie, "Limb amputation and limb deficiency: Epidemiology and recent trends in the United States," *South Med. J.*, vol. 95, no. 8, pp. 875–883, Aug. 2002.

[4] A. Branner, R. B. Stein, and E. Fernandez *et al.*, "Long-term stimulation and recording with a penetrating microelectrode array in cat sciatic nerve," *IEEE Trans. Biomed. Eng.*, vol. 51, no. 1, pp. 146–157, Jan. 2004.

[5] R. J. Vetter, J. C. Williams, and J. F. Hetke *et al.*, "Chronic neural recording using silicon-substrate microelectrode arrays implanted in cerebral cortex," *IEEE Trans. Biomed. Eng.*, vol. 51, no. 6, pp. 896–904, Jun. 2004.

[6] X. Liu, D. B. McCreery, and R. R. Carter *et al.*, "Stability of the interface between neural tissue and chronically implanted intracortical microelectrodes," *IEEE Trans. Rehabil. Eng.*, vol. 7, no. 3, pp. 315–326, Sep. 1999.

[7] J. B. Hijjawi, T. A. Kuiken, and R. D. Lipschutz *et al.*, "Improved myoelectric prosthesis control accomplished using multiple nerve transfers," *Plast. Reconstr. Surg.*, vol. 118, no. 7, pp. 1573–1578, Dec. 2006.

[8] T. A. Kuiken, P. D. Marasco, and B. A. Lock *et al.*, "Redirection of cutaneous sensation from the hand to the chest skin of human amputees with targeted reinnervation," *Proc. Nat. Acad. Sci. USA*, vol. 104, no. 50, pp. 20061–20066, Dec. 11, 2007.

[9] L. A. Miller, K. A. Stubblefield, and R. D. Lipschutz *et al.*, "Improved myoelectric prosthesis control using targeted reinnervation surgery: A case series," *IEEE Trans. Neural Syst. Rehabil. Eng.*, vol. 16, no. 1, pp. 46–50, Feb. 2008.

[10] D. K. Leventhal and D. M. Durand, "Chronic measurement of the stimulation selectivity of the flat interface nerve electrode," *IEEE Trans. Biomed. Eng.*, vol. 51, no. 9, pp. 1649–1658, Sep. 2004.

[11] D. Durand, H. J. Park, and B. Wodlinger, "Models of the peripheral nerves for detection and control of neural activity," in *Proc. IEEE Eng. Med. Biol. Soc. Conf.*, 2009, vol. 2009, pp. 3326–3329.

[12] L. R. Hochberg, M. D. Serruya, and G. M. Friehs *et al.*, "Neuronal ensemble control of prosthetic devices by a human with tetraplegia," *Nature*, vol. 442, no. 7099, pp. 164–171, Jul. 13, 2006.

[13] R. A. Normann, "Technology insight: Future neuroprosthetic therapies for disorders of the nervous system," *Nat. Clin. Pract. Neurol.*, vol. 3, no. 8, pp. 444–452, Aug. 2007.

[14] N. A. Fitzsimmons, W. Drake, and T. L. Hanson *et al.*, "Primate reaching cued by multichannel spatiotemporal cortical microstimulation," *J. Neurosci.*, vol. 27, no. 21, pp. 5593–5602, May 23, 2007.

[15] G. S. Dhillon, S. M. Lawrence, and D. T. Hutchinson *et al.*, "Residual function in peripheral nerve stumps of amputees: Implications for neural control of artificial limbs," *J. Hand Surg. Am.*, vol. 29, no. 4, pp. 605–615, Jul. 2004.

[16] S. Micera, L. Citi, and J. Rigosa *et al.*, "Decoding information from neural signals recorded using intraneural electrodes: Toward the development of a neurocontrolled hand prosthesis," *Proc. IEEE*, vol. 98, no. 3, pp. 407–417, Mar. 2010.

[17] S. Raspopovic, M. Capogrosso, and S. Micera, "A computational model for the stimulation of rat sciatic nerve using a transverse intrafascicular multichannel electrode," *IEEE Trans. Neural Syst. Rehabil. Eng.*, vol. 19, no. 4, pp. 333–344, Aug. 2011.

[18] R. Biran, D. C. Martin, and P. A. Tresco, "Neuronal cell loss accompanies the brain tissue response to chronically implanted silicon microelectrode arrays," *Exp. Neurol.*, vol. 195, no. 1, pp. 115–126, Sep. 2005.

[19] R. Biran, D. C. Martin, and P. A. Tresco, "The brain tissue response to implanted silicon microelectrode arrays is increased when the device is tethered to the skull," *J. Biomed. Mater. Res. A*, vol. 82, no. 1, pp. 169–178, Jul. 2007.

[20] B. K. Leung, R. Biran, and C. J. Underwood *et al.*, "Characterization of microglial attachment and cytokine release on biomaterials of differing surface chemistry," *Biomaterials*, vol. 29, no. 23, pp. 3289–3297, Aug. 2008.

[21] J. C. Williams, J. A. Hippensteel, and J. Dilgen *et al.*, "Complex impedance spectroscopy for monitoring tissue responses to inserted neural implants," *J. Neural Eng.*, vol. 4, no. 4, pp. 410–423, Dec. 2007.

[22] K. Garde, E. W. Keefer, and B. Botterman *et al.*, "Early interfaced neural activity from chronic amputated nerves," *Front. Neuroeng.*, vol. 2, no. 5, pp. 1–11, 2009.

[23] M. Makwana and G. Raivich, "Molecular mechanisms in successful peripheral regeneration," *FEBS J.*, vol. 272, no. 11, pp. 2628–2638, Jun. 2005.

[24] G. C. McConnell, R. J. Butera, and R. V. Bellamkonda, "Bioimpedance modeling to monitor astrocytic response to chronically implanted electrodes," *J. Neural Eng.*, vol. 6, no. 5, p. 055005, Oct. 2009.

[25] I. A. McKenzie, J. Biernaskie, and J. G. Toma *et al.*, "Skin-derived precursors generate myelinating Schwann cells for the injured and dysmyelinated nervous system," *J. Neurosci.*, vol. 26, no. 24, pp. 6651–6660, Jun. 14, 2006.

[26] D. McDonald, C. Cheng, and Y. Chen *et al.*, "Early events of peripheral nerve regeneration," *Neuron Glia Biol.*, vol. 2, no. 2, pp. 139–147, May 2006.

[27] Y. Y. Chen, D. McDonald, and C. Cheng *et al.*, "Axon and Schwann cell partnership during nerve regrowth," *J. Neuropathol. Exp. Neurol.*, vol. 64, no. 7, pp. 613–622, Jul. 2005.

[28] S. M. Hall, "Regeneration in cellular and acellular autografts in the peripheral nervous system," *Neuropathol. Appl. Neurobiol.*, vol. 12, no. 1, pp. 27–46, Jan.-Feb. 1986.

[29] Z. Dong, A. Brennan, and N. Liu *et al.*, "Neu differentiation factor is a neuron-glia signal and regulates survival, proliferation, and maturation of rat Schwann cell precursors," *Neuron*, vol. 15, no. 3, pp. 585–596, Sep. 1995.

[30] C. Taveggia, G. Zanazzi, and A. Petrylak *et al.*, "Neuregulin-1 type III determines the ensheathment fate of axons," *Neuron*, vol. 47, no. 5, pp. 681–694, 2005.

[31] G. Lemke and J. Brockes, "Identification and purification of glial growth factor," *J. Neurosci.*, vol. 4, no. 1, pp. 75–83, January 1, 1984.

[32] K.-A. Nave and J. L. Salzer, "Axonal regulation of myelination by neuregulin 1," *Current Opin. Neurobiol.*, vol. 16, no. 5, pp. 492–500, 2006.

[33] G. Zanazzi, S. Einheber, and R. Westreich *et al.*, "Glial growth factor/neuregulin inhibits schwann cell myelination and induces demyelination," *J. Cell Biol.*, vol. 152, no. 6, pp. 1289–1300, March 19, 2001.

[34] J. M. Le Beau, H. C. Powell, and M. H. Ellisman, "Node of Ranvier formation along fibres regenerating through silicone tube implants: A freeze-fracture and thin-section electron microscopic study," *J. Neurocytol.*, vol. 16, no. 3, pp. 347–358, 1987.

[35] J. H. Caldwell, K. L. Schaller, and R. S. Lasher *et al.*, "Sodium channel Nav1.6 is localized at nodes of Ranvier, dendrites, and synapses," *Proc. Nat. Acad. Sci.*, vol. 97, no. 10, pp. 5616–5620, May 9, 2000.

[36] J. Roper and J. R. Schwarz, "Heterogeneous distribution of fast and slow potassium channels in myelinated rat nerve fibres," *J. Physiol.*, vol. 416, no. 1, pp. 93–110, Sep. 1, 1989.

Jennifer L. Seifert received the Ph.D. degree in molecular biology from Texas Woman's University, Denton, in 2008. Her postdoctoral work at the University of Texas at Arlington included the establishment of an animal model of distraction spinal cord injury and peripheral nerve interfacing.

In 2011, she joined the research faculty in the Department of Bioengineering at the University of Texas at Arlington. Her current research interests include cellular and molecular mechanisms of spinal cord injury and neuroprotection, axon growth and guidance and peripheral neurointerfaces.

Vidhi Desai, photograph and biography not available at the time of publication.

Robert C. Watson, photograph and biography not available at the time of publication.

Tabassum Musa, photograph and biography not available at the time of publication.

Young-tae Kim received the Ph.D. degree in bioengineering from the University of Utah, Salt Lake City, in 2004. In his postdoctoral works at Georgia Institute of Technology, Atlanta, he worked in two areas of nervous system clinical treatment after injury: neuronal protection after spinal cord injury and peripheral nerve regeneration after peripheral nerve injury using an aligned nanofiber based construct.

In 2007, he joined the University of Texas at Arlington as an Assistant Professor of Bioengineering. His research focuses on peripheral nerve injury, regeneration, and interface; microfluidic enabled nerve injury and regeneration; and engineering enabled neuro-oncology for brain cancer treatment.

Edward W. Keefer, photograph and biography not available at the time of publication.

Mario I. Romero-Ortega (M'11) received the Ph.D. degree in neuroscience in 1997 from Tulane University, New Orleans, LA, and postdoctoral training in gene transfer and developmental biology at University of Texas Southwestern Medical Center, Dallas.

In 2002, he became the Director of the Regenerative Neurobiology Research Division at Texas Scottish Rite Hospital for Children and Assistant Professor of Neurology and Plastic Surgery at University of Texas Southwestern Medical Center. In 2008 he joined the University of Texas at Arlington as Associate Professor of Bioengineering. His research focuses in the general area of spinal cord injury monitoring and neuroprotection, peripheral nerve gap injury repair, and regenerative peripheral neuro interfaces.